

placed at a distance of 2 m and listeners could use four intervals (centred at 0, 1, 2 and 3 m) for their distance judgements. Because the low number of intervals could have affected the results (owing to the limited resolution and the possible occurrence of end effects), the interval number was doubled in the second experiment (intervals were now centred at 0–3.5 m in 0.5-m steps). In addition, the loudspeaker was moved to a distance of 3 m to check whether its position had introduced a bias. The 3-m gap was bridged by two poles, placed at distances of 1 and 2 m, that provided additional reference points. Six listeners participated in each experiment. A between-groups analysis of variance, applied to results of the two experiments, showed that the results for the conditions that were replicated did not differ significantly ($P = 0.73$). Thus, results were affected neither by the number of intervals nor by the position of the loudspeaker.

Received 3 December; accepted 21 December 1998.

1. Békésy, G. v. Über die Entstehung der Entfernungsempfindung beim Hören. *Akustische Z.* **3**, 21–31 (1938).
2. Mershon, D. H. & King, L. E. Intensity and reverberation as factors in the auditory perception of egocentric distance. *Percept. Psychophys.* **18**, 409–415 (1975).
3. Mershon, D. H. & Bowers, J. N. Absolute and relative cues for the auditory perception of egocentric distance. *Perception* **8**, 311–322 (1979).
4. Nielsen, S. H. Auditory distance perception in different rooms. *J. Audio Eng. Soc.* **41**, 755–770 (1993).
5. Wightman, F. L. & Kistler, D. J. Headphone simulation of free-field listening: II. Psychophysical validation. *J. Acoust. Soc. Am.* **85**, 868–878 (1989).
6. Bronkhorst, A. W. Localization of real and virtual sound sources. *J. Acoust. Soc. Am.* **98**, 2542–2553 (1995).
7. Houtgast, T. & Aoki, S. Stimulus-onset dominance in the perception of binaural information. *Hearing Res.* **72**, 29–36 (1994).
8. Coleman, P. D. Failure to localize the source distance of an unfamiliar sound. *J. Acoust. Soc. Am.* **34**, 345–346 (1962).
9. Coleman, P. D. An analysis of cues to auditory distance perception in free space. *Psychol. Bull.* **60**, 302–315 (1963).
10. Blauert, J. *Spatial Hearing* (MIT Press, Cambridge, Massachusetts, 1997).
11. Begault, D. R. Perceptual effects of synthetic reverberation on three-dimensional audio systems. *J. Audio Eng. Soc.* **40**, 895–904 (1992).
12. Moore, B. C. J., Glasberg, B. R., Plack, C. J. & Biswas, A. K. The shape of the ear's temporal window. *J. Acoust. Soc. Am.* **83**, 1102–1116 (1988).
13. Kuttruff, H. *Room Acoustics* (Applied Science, London, 1973).
14. Wetschurack, R., Plenge, G. & Lehringer, F. Entfernungswahrnehmung beim natürlichen Hören sowie bei kopfbezogenen Stereophonie. *Acustica* **29**, 260–272 (1973).
15. Møller, H., Sørensen, M. F., Hammershoi, D. & Jensen, C. B. Head-related transfer functions of human subjects. *J. Audio Eng. Soc.* **43**, 300–321 (1995).

Acknowledgements. Part of this research was done within the European AUDIS project.

Correspondence and requests for materials should be addressed to A.W.B. (e-mail: bronkhorst@tm.tno.nl)

The arrangement of the three cone classes in the living human eye

Austin Roorda*† & David R. Williams*

*Center for Visual Science, University of Rochester, Rochester, New York 14627, USA

Human colour vision depends on three classes of receptor, the short- (S), medium- (M), and long- (L) wavelength-sensitive cones. These cone classes are interleaved in a single mosaic so that, at each point in the retina, only a single class of cone samples the retinal image. As a consequence, observers with normal trichromatic colour vision are necessarily colour blind on a local spatial scale¹. The limits this places on vision depend on the relative numbers and arrangement of cones. Although the topography of human S cones is known^{2,3}, the human L- and M-cone submosaics have resisted analysis. Adaptive optics, a technique used to overcome blur in ground-based telescopes⁴, can also overcome blur in the eye, allowing the sharpest images ever taken of the living retina⁵. Here we combine adaptive optics and retinal densitometry⁶ to obtain what are, to our knowledge, the first images of the arrangement of S, M and L cones in the living human eye. The proportion of L to M cones is strikingly different in two male subjects, each of whom has normal colour vision. The

mosaics of both subjects have large patches in which either M or L cones are missing. This arrangement reduces the eye's ability to recover colour variations of high spatial frequency in the environment but may improve the recovery of luminance variations of high spatial frequency.

We measured the eye's aberrations with a Hartmann–Shack wavefront sensor and compensated for them with a deformable mirror (see ref. 4 for details). We then collected images of the cone mosaic, as shown in Fig. 1a, with a charge-coupled device (CCD). Individual cones were classified by comparing images taken when the photopigments were fully bleached with those taken when the photopigments were either dark-adapted or exposed to a light that selectively bleached one photopigment. From these images, we created absorbance images that remove static features to reveal only the distribution of the photolabile pigments that distinguish the cone classes.

To distinguish S cones from M and L cones, we obtained absorbance images from dark-adapted and fully bleached images.

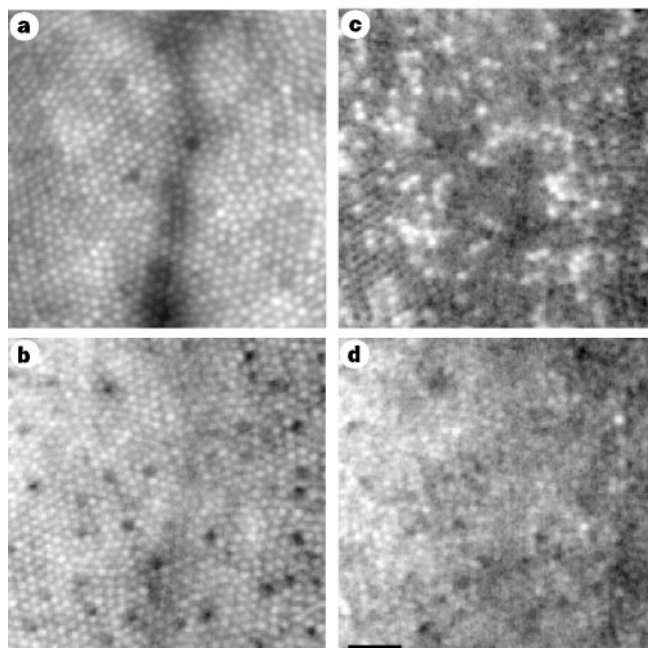


Figure 1 Images of the right eye of subject JW. The mosaic was illuminated with a 4-ms flash (1 degree diameter, $\sim 0.3 \mu\text{J}$) through a 2-mm entrance pupil. Light of wavelength 550 nm was used to maximize absorbance by L- and M-cone photopigment. Images were obtained with a 6-mm exit pupil at a retinal eccentricity of one degree nasal from the foveal centre, which is located to the left of the image. For each retinal location, about 50 images taken over 5 days were averaged to increase the signal-to-noise ratio. Fixational eye movements translate the image from flash to flash, requiring registration with cross-correlation before averaging. **a**, A registered sum of 61 images taken after a full bleach. **b–d**, Absorbance images of the patch of cones shown in **a**, defined as 1 minus the ratio of the absorbance of a dark-adapted or selectively bleached image to the absorbance of the corresponding fully bleached image. Images of fully bleached retina were obtained following exposure to 550-nm light (70-nm bandwidth, 37×10^6 troland-seconds). Images of dark-adapted retina were taken following 5 min of dark adaptation. **b**, The absorbance image of dark-adapted cones, revealing a sparse array of S cones which appear dark because of their low absorbance at 550 nm. **c, d**, Absorbance images following a 470-nm (**c**) and 650-nm (**d**) selective bleach. Bleaching energies were set by calculation and then modified empirically to achieve the maximum possible difference between M- and L-photopigment concentration. The absorbance images for both bleaching conditions have higher pigment density toward the fovea; this is caused by the increases in the length of the outer segment and in macular pigment, which reduce bleaching in the 470-nm condition. Scale bar represents 5 arcmin of visual angle.

†Present address: University of Houston, College of Optometry, Houston, Texas 77204-6052, USA

Because S cones absorb negligibly at the imaging wavelength of 550 nm, whereas M and L cones absorb strongly at this wavelength, the S cones appear as a sparse array of dark cones in the absorbance image of Fig. 1b while the M and L cones appear bright. To distinguish L from M cones, we took images immediately after one of two bleaching conditions: dark-adapted retina was exposed to a 650-nm light, which selectively bleached the L pigment, or a 470-nm light, which selectively bleached the M pigment. The absorbance image for the 650-nm bleach reveals dark, low-absorbance L cones that have been heavily bleached and bright, highly absorbing M cones that were spared from bleaching (Fig. 1c). The absorbance image for the 470-nm bleach shows selective bleaching of M cones, but the effect is smaller than the effect of the 650-nm bleach because of the similarity of M-cone and L-cone action spectra at this wavelength (Fig. 1d).

Figure 2a–d shows that, for two trichromats with normal colour vision, the absorbances of single cones after 470-nm and 650-nm bleaches produce a bimodal distribution. If these modes represent L and M cones, then only a single mode should be observed in a similar experiment on a protanope, a person who lacks the L pigment. This prediction is confirmed by the data shown in Fig. 2e, f. Table 1 summarizes the numbers of S, M and L cones found in the two trichromats. The relative number of L and M cones differs greatly between these two subjects. In two patches of retina, one from the nasal and one from the temporal fovea, subject JW had a mean ratio of L to M cones of 3.79 whereas AN had a ratio of 1.15. This large individual difference is consistent with the variability found using psychophysical methods^{7–10}, spectral electroretinograms^{11,12}, microspectrophotometry^{13,14} and messenger RNA analysis^{15,16}.

The arrangements of S, M and L cones for subjects JW and AN are shown in the pseudocolour images in Fig. 3. The distribution of the sparse S cones is not significantly different from random in either trichromat. This agrees with previous results³ that showed that the developmental mechanism used to space S cones in a regular,

Table 1 Cone numbers for two subjects with normal colour vision

Subject	Number of cones	L cones (%)	M cones (%)	S cones (%)	Error (%)	L:M ratio
JW	1462	75.8	20.0	4.2	2.1	3.79
AN	522	50.6	44.2	5.2	5.6	1.15

The error column shows the percentage of cones labelled M (or L) that are actually L (or M) cones. The error in the assignment of L and M cones is taken to be the fractional area of the intersection of the sum of two gaussians used to fit the histograms shown in Fig. 2.

nonrandom manner in humans is not seen near the fovea. Perhaps cone migration during the formation of the fovea disrupts regular S-cone spacing. The assignment of M and L cones is not significantly different from random in JW's eye but in AN's eye the M and L cones are significantly more aggregated than expected in a random mosaic. This additional clumping could arise if, for example, progenitor cells were to bias the 'decisions' of their progeny to express either M or L opsin. However, we cannot exclude the possibility that the departure from a random distribution in AN's eye is a consequence of residual optical blur in his retinal images. Optical blur could increase the chances of misclassifying especially those cones that are surrounded by cones of the opposite class, and this would exaggerate clumping. The overlap in the two distributions of Fig. 2d indicates that about 6% of AN's M and L cones were misidentified. Simulations suggest that this low error rate may nonetheless be high enough to produce the tendency towards the additional clumping we observed. Microspectrophotometry¹⁷ on small foveal patches of excised talapoin retina indicated a random assignment of M and L cones and photopigment transmittance imaging in a macaque peripheral retina¹⁸ showed a tendency towards aggregation of M and L cones. All studies agree that there is no tendency for the M cones to disperse themselves uniformly among the L cones, and the lack of a regular packing scheme for these cone classes may be ubiquitous among old-world primates.

What are the implications of this arrangement for vision? The coarse grain of the cone submosaics causes fluctuations in the

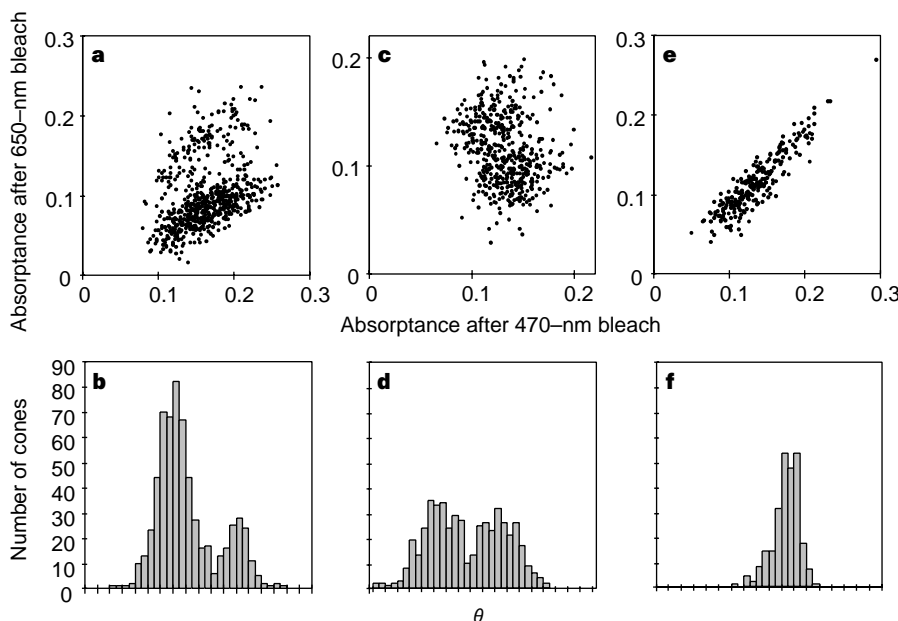


Figure 2 Scatter plots and histograms of individual cone absorbances. Scatter plots show the absorbance of each cone in a contiguous patch after the 470-nm and 650-nm selective bleaches. Cone absorbance was taken as the average value computed within a 0.4-arcmin square region centred on the cone. Histograms show the distribution of cones as a function of angle (θ) in the scatter plots. **a, b**, Results derived from the absorbance images of Fig. 1c, d, with S cones removed. **c, d**, Results obtained from a second trichromat, AN. For these trichromats, we fitted the sum of two gaussian curves to the histograms. The

angle corresponding to the intersection of the two gaussian curves was used to categorize L and M cones. The fractional area of the overlap compared with the total area under the two gaussians provides an estimate of the fraction of cones that were misidentified; these estimates are 2.1% for JW and 5.6% for AN. **e, f**, Results obtained from a protanope whose colour deficiency was verified psychophysically and by genetic screening. As with the trichromats, bleaching levels were chosen to optimize the chance of distinguishing two pigments.

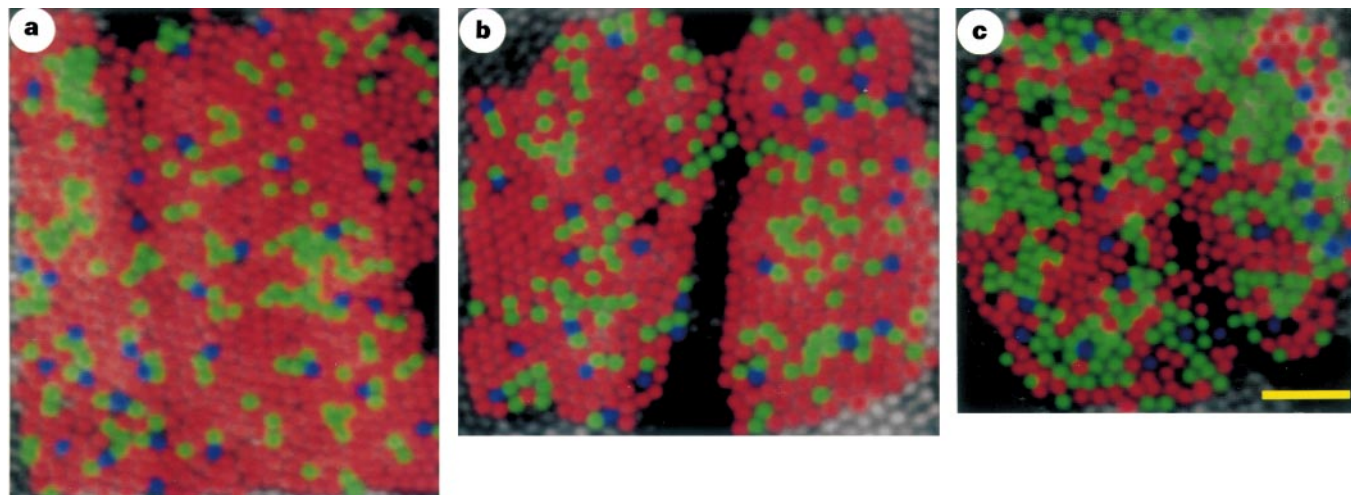


Figure 3 Pseudocolour image of the trichromatic cone mosaic. Blue, green and red colours represent the S, M and L cones, respectively. **a, b**, Subject JW's temporal and nasal retina, respectively, at one degree of eccentricity. **c**, Subject AN's nasal retina, at one degree of eccentricity. We performed a statistical test for randomness according to Diggle²⁷. We compared the distribution of all intercone distances of the measured M-cone array with 100 simulations derived from the

same mosaic in which the same number of M cones were randomly assigned. JW's array was no different from random at either location. AN's array showed significant clumping of the data ($P < 0.01$) but, because of optical blur, the possibility of a random assignment of M cones cannot be ruled out. Scale bar represents 5 arcmin of visual angle.

colour appearance of tiny, monochromatic light flashes^{19,20} because the relative excitation of different cone classes depends on the location of the flash. A related illusion is Brewster's colours, the perception of irregular patches of pastel colour while viewing periodic black and white patterns of high spatial frequency^{1,21}. Similarly, red-green isoluminant gratings with spatial frequencies above the resolution limit look like chromatic and luminant spatial noise²². All of these perceptual errors are examples of the aliasing produced when the three cone submosaics sample the retinal image inadequately. They are akin to the errors that occur in images taken with digital cameras that have interleaved pixels of different spectral sensitivity¹. The clumping that results from either the random or the aggregated assignment of M and L cones exacerbates these errors.

Both of our subjects have retinal patches of 5 arcmin or more across that contain only one of the two longer-wavelength-sensitive cone classes. Although the existence of these patches indicates that the trichromat may sometimes misjudge the colour appearance of tiny objects, the patches will be beneficial in recovering high-frequency luminance patterns, because cortical neurons tuned to high spatial frequency are more likely to be fed by contiguous cones of the same class. This may explain the observation that, in some normal trichromats, there is little or no difference in resolution for gratings seen with only M cones or only L cones, or when both cone classes operate together²³. Only when one cone class is greatly under-represented, as occurs in some heterozygous carriers for congenital X-linked protanopia, is resolution clearly mediated by the more dense submosaic²⁴.

The large individual differences in numbers and arrangement of cone classes that we have observed indicate that evolution has not converged on an optimum proportion of M and L cones for the human eye. Is this because red-green colour vision is a relatively new feature of vision in old-world primates^{25,26}, or do the statistics of natural scenes, optical blurring and clever post-receptor processing make M- and L-cone topography unimportant for visual performance? The imaging method described here allows us to address these questions, because it is now possible to assess visual performance and the circuitry of the retina in eyes for which the trichromatic mosaic is known. □

Received 16 October; accepted 26 November 1998.

1. Williams, D. R., Sekiguchi, N., Haake, W., Brainard, D. H. & Packer, O. S. in *From Pigments to Perception*. (eds Valberg, A. & Lee, B. B.) 11–22 (Plenum, New York, 1991).

2. Williams, D. R., MacLeod, D. I. A. & Hayhoe, M. Punctate sensitivity of the blue sensitive mechanism. *Vision Res.* **21**, 1357–1375 (1981).
3. Curcio, C.A. *et al.* Distribution and morphology of human cone photoreceptors stained with anti-blue opsin. *J. Comp. Neurol.* **312**, 610–624 (1991).
4. Babcock, H.W. The possibility of compensating astronomical seeing. *Publ. Astron. Soc. Pacif.* **65**, 229–236 (1953).
5. Liang, J., Williams, D. R. & Miller, D. T. Supernormal vision and high-resolution retinal imaging through adaptive optics. *J. Opt. Soc. Am. A* **14**, 2884–2892 (1997).
6. Campbell, F. W. & Rushton, W. A. H. Measurement of the scotopic pigment in the living human eye. *J. Physiol. (Lond.)* **130**, 131–147 (1955).
7. Rushton, W. A. H. & Baker, H. D. Red/green sensitivity in normal vision. *Vision Res.* **4**, 75–85 (1964).
8. Pokorny, J., Smith, V. C. & Wesner, M. in *From Pigments to Perception* (eds Valberg, A. & Lee, B. B.) 23–34 (Plenum, New York, 1991).
9. Cicerone, C. M. & Nerger, J. L. The relative numbers of long-wavelength-sensitive to middle-wavelength-sensitive cones in the human fovea. *Vision Res.* **26**, 115–128 (1989).
10. Vimal, R. L. P., Pokorny, J., Smith, V. C. & Shevell, S. K. Foveal cone thresholds. *Vision Res.* **29**, 61–78 (1989).
11. Jacobs, G. H. & Neitz, J. in *Colour Vision Deficiencies* Vol. XI (ed. Drum, B.) 107–112 (Kluwer Academic, Netherlands, 1993).
12. Jacobs, G. H. & Deegan, J. F. Spectral sensitivity of macaque monkeys measured with ERG flicker photometry. *Vis. Neurosci.* **14**, 921–928 (1997).
13. Bowmaker, J. K. & Dartnall, H. J. A. Visual pigments of rods and cones in a human retina. *J. Physiol. (Lond.)* **298**, 501–511 (1980).
14. Dartnall, H. J. A., Bowmaker, J. K. & Mollon, J. D. Human visual pigments: microspectrophotometric results from the eyes of seven persons. *Proc. R. Soc. Lond. B* **220**, 115–130 (1983).
15. Yamaguchi, T., Motulsky, A. G. & Deeb, S. S. Visual pigment gene structure and expression in human retinae. *Hum. Mol. Genet.* **6**, 981–990 (1998).
16. Hagstrom, S. A., Neitz, J. & Neitz, M. Variation in cone populations for red-green color vision examined by analysis of mRNA. *NeuroReport* **9**, 1963–1967 (1998).
17. Mollon, J. D. & Bowmaker, J. K. The spatial arrangement of cones in the primate fovea. *Nature* **360**, 677–679 (1992).
18. Packer, O. S., Williams, D. R. & Bensinger, D. G. Photoreceptor transmittance imaging of the primate photoreceptor mosaic. *J. Neurosci.* **16**, 2251–2260 (1996).
19. Holmgren, E. Uber den Farbensinn. *Comp. Rend. Congr. Period. Intern. Sci. Med. Copenhagen* **1**, 80–98 (1884).
20. Krauskopf, J. Color appearance of small stimuli and the spatial distribution of color receptors. *J. Opt. Soc. Am.* **54**, 1171 (1964).
21. Brewster, D. On the undulations excited in the retina by the action of luminous points and lines. *Lond. Edinb. Philos. Mag. J. Sci.* **1**, 169–174 (1832).
22. Sekiguchi, N., Williams, D. R. & Brainard, D. H. Efficiency in detection of isoluminant and isochromatic interference fringes. *J. Opt. Soc. Am. A* **10**, 2118–2133 (1993).
23. Williams, D. R. in *Advances in Photoreception: Proc. Symp. Frontiers Visual Sci.* 135–148 (National Academy, Washington DC, 1990).
24. Miyahara, E., Pokorny, J., Smith, V. C., Baron, R. & Baron, E. Color vision in two observers with highly biased LWS/MWS cone ratios. *Vision Res.* **38**, 601–612 (1998).
25. Nathans, J., Thomas, D. & Hogness, D. S. Molecular genetics of human colour vision: the genes encoding blue, green and red pigments. *Science* **232**, 193–202 (1986).
26. Mollon, J. D. "Tho' she kneeled in that place where they grew...": The uses and origins of primate colour vision. *J. Exp. Biol.* **146**, 21–38 (1989).
27. Diggle, P. J. *Statistical Analysis of Spatial Point Patterns* (Academic, London, 1983).

Acknowledgements. We thank D. Brainard, D. Dacey, J. Jacobs, J. Liang, D. Miller and O. Packer for their assistance. We acknowledge financial support from the Fight for Sight research division of Prevent Blindness America (to A.R.) and the National Eye Institute and Research to Prevent Blindness (to D.R.W.).

Correspondence and requests for materials should be addressed to A.R. (e-mail: aroorda@popmail.opt.uh.edu).